Journal of Biomedical Optics

BiomedicalOptics.SPIEDigitalLibrary.org

Video-rate *in vivo* fluorescence imaging with a line-scanned dual-axis confocal microscope

Ye Chen
Danni Wang
Altaz Khan
Yu Wang
Sabine Borwege
Nader Sanai
Jonathan T. C. Liu

SPIE.

Video-rate *in vivo* fluorescence imaging with a line-scanned dual-axis confocal microscope

Ye Chen,[a,*,†] Danni Wang,[b,†] Altaz Khan,[b] Yu Wang,[a] Sabine Borwege,[c] Nader Sanai,[c] and Jonathan T. C. Liu[a]
[a]University of Washington, Department of Mechanical Engineering, Molecular Biophotonics Laboratory, Seattle, Washington 98195, United States
[b]Stony Brook University, Department of Biomedical Engineering, Molecular Biophotonics Laboratory, Stony Brook, New York 11794, United States
[c]Barrow Brain Tumor Research Center, Division of Neurosurgical Oncology, Barrow Neurological Institute, St. Joseph's Hospital and Medical Center, Phoenix, Arizona 85013, United States

Abstract. Video-rate optical-sectioning microscopy of living organisms would allow for the investigation of dynamic biological processes and would also reduce motion artifacts, especially for *in vivo* imaging applications. Previous feasibility studies, with a slow stage-scanned line-scanned dual-axis confocal (LS-DAC) microscope, have demonstrated that LS-DAC microscopy is capable of imaging tissues with subcellular resolution and high contrast at moderate depths of up to several hundred microns. However, the sensitivity and performance of a video-rate LS-DAC imaging system, with low-numerical aperture optics, have yet to be demonstrated. Here, we report on the construction and validation of a video-rate LS-DAC system that possesses sufficient sensitivity to visualize fluorescent contrast agents that are topically applied or systemically delivered in animal and human tissues. We present images of murine oral mucosa that are topically stained with methylene blue, and images of protoporphyrin IX-expressing brain tumor from glioma patients that have been administered 5-aminolevulinic acid prior to surgery. In addition, we demonstrate *in vivo* fluorescence imaging of red blood cells trafficking within the capillaries of a mouse ear, at frame rates of up to 30 fps. These results can serve as a benchmark for miniature *in vivo* microscopy devices under development. [DOI: 10.1117/1.JBO.20.10.106011]

Keywords: dual-axis confocal microscopy; line scanning; fluorescence imaging; *in vivo* imaging; video-rate imaging.

Paper 150408R received Jun. 16, 2015; accepted for publication Sep. 30, 2015; published online Oct. 28, 2015.

1 Introduction

While microscopy of *ex vivo* tissues provides valuable information for biological investigations and clinical diagnoses, key insights into dynamic processes can only be obtained under *in vivo* settings. Video-rate microscopy (defined here as ≥15 fps) has shown utility for visualizing cellular-level dynamics, such as blood cells trafficking within capillary networks.[1–4] In addition, high-frame-rate microscopy is useful for mitigating motion artifacts due to respiration or mechanical jitter when utilizing an intravital, handheld, or endoscopic microscope.[5–9]

In recent years, considerable efforts have been undertaken to develop miniature optical-sectioning microscopes for applications such as *in vivo* microendoscopy and point-of-care pathology.[5,10–22] Regardless of the specific modality—e.g., confocal microscopy, optical coherence tomography, photoacoustic tomography, or multiphoton microscopy—a general goal has been to maximize the imaging depth, resolution, contrast, field of view (FOV), and speed of imaging. In practice, various trade-offs are necessary to optimize a device for a particular application. Among various methods, a number of miniature microscopes have been developed that utilize a point-scanned dual-axis confocal configuration (PS-DAC).[23–25] A DAC microscope is a unique confocal architecture that utilizes low-numerical aperture (NA) off-axis illumination and collection beams that intersect precisely at their foci. The DAC architecture decreases the undesired background from multiplying scattered and out-of-focus photons, which in turn improves imaging contrast and depth compared to a conventional single-axis confocal microscope.[26] Point-scanned confocal microscopes achieve optical sectioning through spatial filtering with a pinhole detector, in which an image is obtained in a point-by-point fashion by mechanically scanning the sample or by scanning the focal volume within the sample. However, with frame rates that are typically lower than 10 Hz, the images obtained by a point-scanned confocal microscope are often susceptible to motion artifacts.[27] In addition, such slow frame rates (<10 Hz) are lower than the frequency response of the human visual system (~15 Hz) when perceiving moving objects.[28]

In order to address the drawback of limited imaging speed, modifications were made to a DAC microscope to accommodate line scanning instead of point scanning. Even though confocality is lost in one dimension for a line-scanned dual-axis confocal (LS-DAC) microscope, which limits its ability to image deeper within tissues, previous feasibility studies have shown that a slow stage-scanned LS-DAC microscope (with 2-fps imaging rate and 1-ms line-acquisition rate) can maintain the resolution and contrast of a PS-DAC microscope at moderate depths of up to several hundred microns.[29] In addition, previous Monte-Carlo simulations suggest that a LS-DAC configuration provides superior contrast (signal to background ratio, SBR) in comparison to a line-scanned single-axis confocal microscope.[30] Recently, we have also introduced a variation on the LS-DAC technique called sheet-scanned dual-axis confocal (SS-DAC) microscopy,[31] in which a scientific complementary metal–oxide–semiconductor (sCMOS) camera enables an oblique light-sheet to be imaged at each scanned position. However, both the previous

*Address all correspondence to: Ye Chen, E-mail: yechen@uw.edu

†These authors contributed equally.

LS-DAC microscope and the recently developed SS-DAC microscope were slow stage-scanned prototypes (frame rate at 2 fps) that did not utilize a fast-scanning galvo (up to 30 Hz), high-speed camera acquisition (10-kHz line acquisition rate), and speed-optimized software. On the other hand, a major challenge for many high-frame-rate fluorescence optical-sectioning devices (with short pixel dwell times) is achieving adequate sensitivity. This is especially true for DAC microscopy, in which low-NA optics are utilized. Here, we demonstrate for the first time that an LS-DAC microscope is capable of achieving video-rate imaging of fluorescently labeled tissues with sufficient sensitivity for a number of potential biological and clinical applications.

The results of this study demonstrate that video-rate LS-DAC microscopy is capable of sensitive *in vivo* video-rate imaging of blood cells trafficking within the capillaries of a mouse ear at 15 fps (FOV $\sim 500 \times 500$ μm) or 30 fps (FOV $\sim 250 \times 500$ μm). In addition, the 100-μs camera exposure time (line-acquisition rate) used for video-rate *in vivo* imaging experiments provides sufficient sensitivity to image excised mouse tongue tissues, topically stained with methylene blue, at subcellular resolution. To further demonstrate the versatility of video-rate LS-DAC microscopy for clinical applications, images are obtained from surgically excised human brain tumor specimens (glioma) expressing 5-aminolevulinic acid (5-ALA)-induced protoporphyrin IX (PpIX) fluorescence.

2 Methods

2.1 *Video-Rate Line-Scanned Dual-Axis Confocal Microscope*

Figure 1 provides a schematic of the optical setup of the high-speed (15 and 30 fps) LS-DAC microscope. In brief, a single-mode fiber-coupled diode laser (658-nm from Coherent Inc., 488-nm from Coherent Inc., or 405-nm from SFOLT Co., Ltd.) was collimated and focused to a ~500-μm-long [full width at half maximum (FWHM)] line in the sample without magnification (Gaussian NA = 0.12). A solid immersion lens (SIL, $n = 1.45$) was used to index match the illumination and collection beams into the sample, increasing the NA of the illumination beam from 0.12 to 0.17. The light from the sample was collected off-axis from the illumination path (with a half-crossing angle of 30 deg), transmitted through a long-pass fluorescence filter (Semrock, LP02-488RU-25 or LP02-664RU) and imaged with 5× magnification ($L2$) onto a sCMOS camera (ORCA flash 4.0 v2, Hamamatsu). A galvanometric scanning mirror (Cambridge Technologies), driven by a custom LabVIEW program (National Instruments), was used to scan the confocal line along the x-axis. Individual confocal image frames were stitched together in a line-by-line fashion using a custom MATLAB® script (Mathworks), and the image stacks were rendered into videos using ImageJ (NIH).

The sCMOS camera used as a detector in this study was able to acquire ~10,000 raw acquisitions (confocal lines) per second at a 100-μs exposure time for a thin rectangular region of interest of 8×2048 pixels. The center 3-pixel width of this strip corresponded to an imaging dimension of ~2.7 μm in the tissue sample (slightly larger than the width of our diffraction-limited focal line) and was binned to create a digital confocal slit.

For each two-dimensional (2-D) image, the scanning mirror was programmed to translate the focal line in the x-direction (see Fig. 1). Serially acquired confocal lines were stitched together, enabling a LS-DAC video imaging rate of 15 fps over a $\sim 500 \times 500$ μm FOV, or a 30 fps video imaging rate over a smaller FOV of $\sim 250 \times 500$ μm. A consistent sampling pitch of ~0.75 μm per pixel (at 100-μs line-acquisition rate) was utilized in the x-direction. According to diffraction theory, the FWHM width of the focal line in tissues is 1.4 μm.[32] Thus, we were sampling the x-direction at approximately the Nyquist frequency.

The sampling density in the y-direction was determined by the pixel pitch in the sCMOS camera, which is 6.5 μm. Taking into account the magnification of the SIL sample holder ($n = 1.45$), as well as the magnification of the collection-side optics (5×), the sampling pitch within tissue was approximately 0.9 μm per pixel. The diffraction-limited FWHM resolution in the y-direction is 1.2 μm.[32] Therefore, we were slightly undersampling the y-direction per Nyquist.

2.2 *System Characterization with Reflective Targets*

The axial response of the video-rate LS-DAC microscope was measured with a flat reflective mirror in a homogeneous scattering phantom, 5% Intralipid ($\mu_s \sim 11$ mm^{-1}), or a nonscattering water sample. To obtain the axial response as a function of defocus (mirror distance from the focal plane), a chrome mirror was translated axially away from the microscope's focal plane ($z = 0$) using a computer-controlled actuator (Newport Corporation, CMA-12CCCL) at a velocity of 0.1 μm/s. Here, the imaging depth is expressed as a nondimensional quantity, "the perpendicular optical length" (L_P), which is the total number of scattering mean free paths on a round-trip path between the tissue surface and the mirror target, $L_P = 2\mu_s d$, where d is the physical depth of the mirror in the imaging media, and μ_s is the scattering coefficient of the media. The axial resolution is defined as the FWHM of the axial-response curve (approximately Gaussian in shape).

The lateral resolution of the video-rate LS-DAC microscope was assessed by imaging a high-resolution reflective 1951 USAF bar target (Edmund Optics, 58-198).

2.3 *In Vivo Video-Rate Fluorescence Imaging*

This study was performed in accordance with an animal use protocol approved by the Institutional Animal Care and Use Committees at Stony Brook University. For *in vivo* imaging, fluorescein isothiocyanate (FITC)-conjugated dextran (Sigma Aldrich, FD2000S, 2000 kDa, 10 mg/mL) was injected retro-orbitally into an anesthetized mouse to highlight its vasculature. The mouse was anesthetized with Avertin (Sigma Aldrich, 2,2,2-tribromoethanol, 20 mg/mL) via intraperitoneal injection at 250 mg/kg body mass. The animal was placed on a custom platform that allowed for the imaging of the vasculature in its ears. The animal remained under anesthesia during the imaging experiments and was immediately euthanized upon the completion of the experiments.

In order to image blood cells trafficking within the capillaries of mouse at various depths beneath the ear skin surface, a computer-controlled actuator (Newport Corporation, CMA-12CCCL) was used to translate the sample stage along the z-axis in 25 μm/s steps. Three-dimensional images of mouse-ear vasculature were constructed by acquiring a stack of horizontal image sections [see Figs. 2(a) and 2(b)]. The laser power for *in vivo* fluorescence imaging of red blood cells trafficking within the capillaries of a mouse ear was ~1.8 mW.

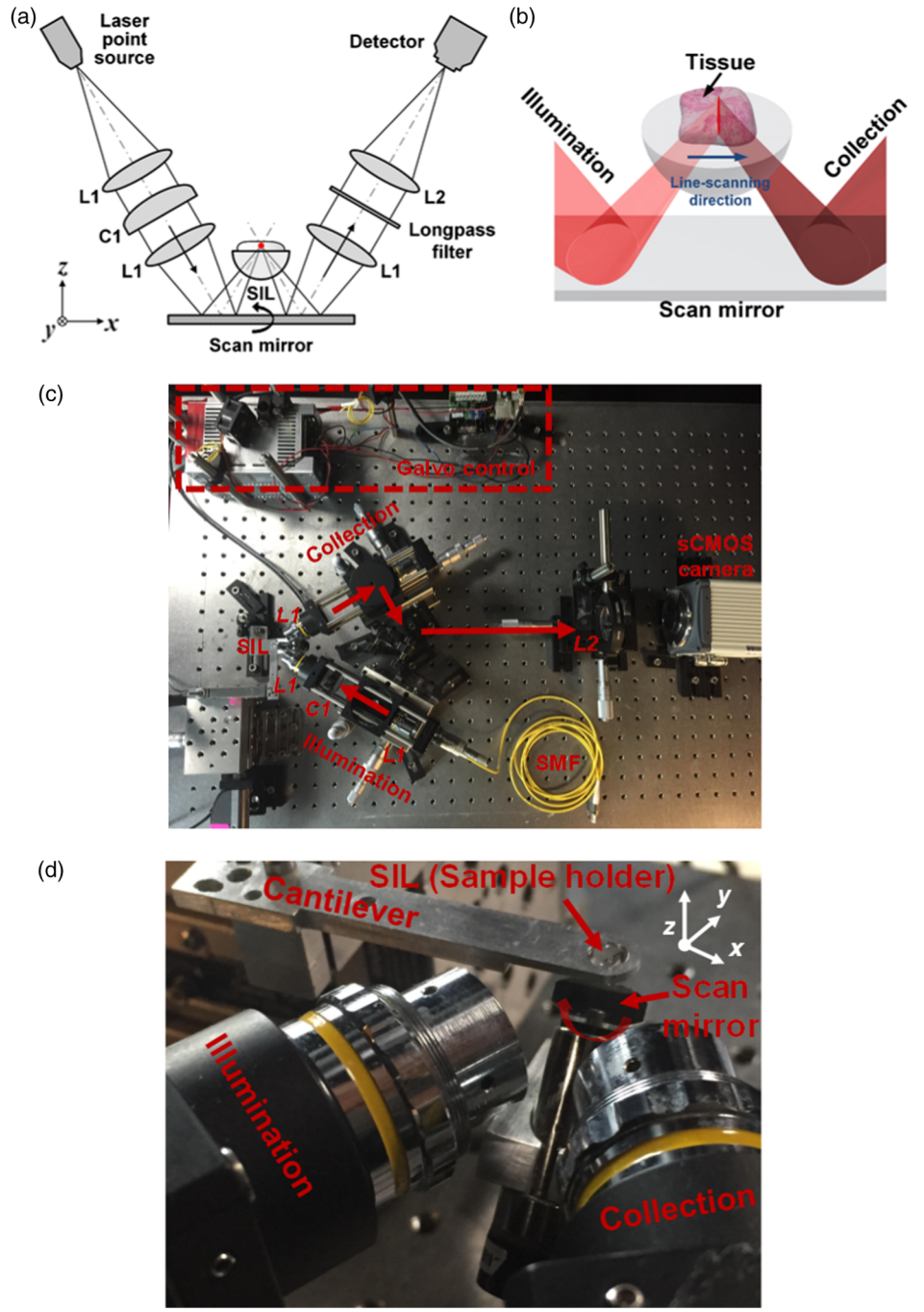

Fig. 1 (a) Schematic of the video-rate line-scanned dual-axis confocal (LS-DAC) microscope. The scan mirror rotates about the *y*-axis and scans the confocal line in the *x*-direction. C1: cylindrical lens. (b) Zoomed-in view of the video-rate LS-DAC microscope near the sample. (c) Photograph of the LS-DAC tabletop implementation. SMF: single-mode fiber. (d) Photograph of the LS-DAC microscope near the focus.

2.4 *Ex Vivo Video-Rate Fluorescence Imaging*

To show that the camera exposure times (100 μs) used for these video-rate *in vivo* imaging experiments could also provide sufficient sensitivity to image both topically applied and systemically delivered fluorescent contrast agents in animal and human tissues, we imaged excised mouse tongue tissues topically stained with methylene blue, as well as PpIX-expressing brain tumors from glioma patients that had been administered 5-ALA prior to surgery. The laser power for *ex vivo* imaging of both mouse tongue and PpIX-expressing human brain tumor was ~1.3 mW.

Excised mouse tongue tissues were topically stained with 0.5 mL of 1% methylene blue (MB) for 10 min and then rinsed thoroughly with 1× PBS. Images were obtained from the top surface of the tongue.

Thick (unsectioned) human brain tumor specimens (low-grade glioma) were obtained during surgery and fixed in 4% paraformaldehyde before being imaged. Prior to surgery,

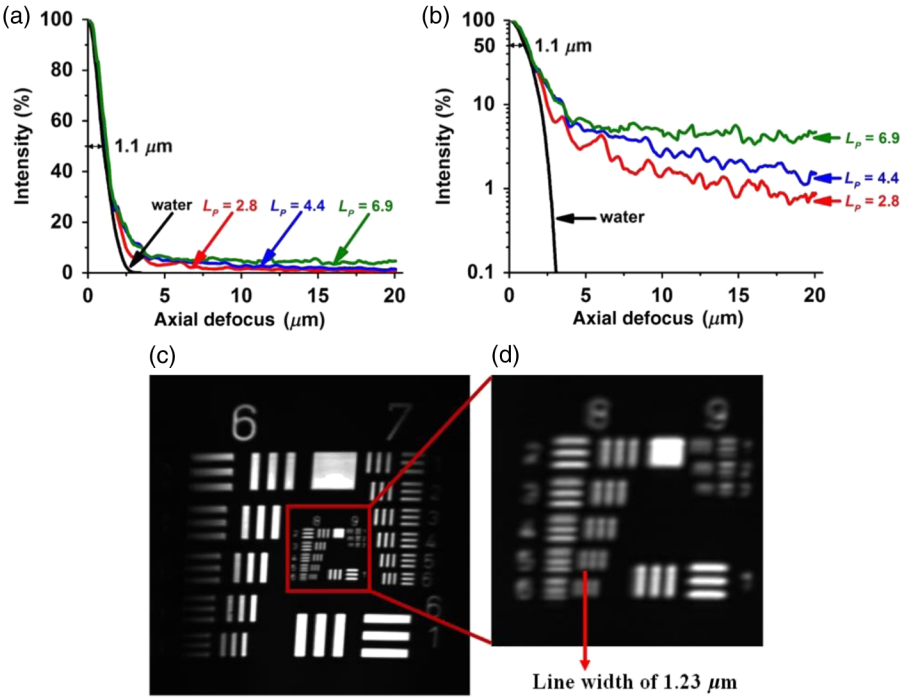

Fig. 2 Axial response of the video-rate LS-DAC microscope to a flat reflective mirror in 5% Intralipid (or water) over a range of optical lengths (L_P) plotted with: (a) a linear scale and (b) a logarithmic scale. The measured half width at half maximum is 1.10 μm. (c) Reflectance image of a 1951 USAF bar target. (d) Zoomed-in view of groups 8 and 9 of the USAF bar target. The video-rate LS-DAC microscope has the ability to resolve group 8, element 5 (line width = 1.23 μm) of the bar target.

5-ALA, a prodrug currently in clinical trials (phase II) for image-guided resection of malignant brain tumor, was orally administered to glioma patients at the Barrow Neurological Institute in Phoenix, Arizona, under an IRB-approved protocol and IND approval for the use of 5-ALA. 5-ALA is intracellularly metabolized by the mitochondria to form PpIX, which has been shown to preferentially accumulate in various tumor cells (including glioma cells).[33] Low-grade gliomas typically do not generate enough PpIX to enable detection using wide-field low-resolution fluorescence imaging, but optical-sectioning confocal microscopy has the resolution and sensitivity to visualize the sparse generation and punctate PpIX expression in these tissues.[34] Here, thick low-grade glioma tissues were imaged with the video-rate LS-DAC microscope to visualize the subcellular PpIX expression (405-nm excitation and 625-nm collection).

3 Results

Our results indicate that video-rate LS-DAC microscopy is capable of *in vivo* fluorescence imaging of blood cells trafficking within the capillaries of a mouse ear at a frame rate of 15 fps (FOV $\sim 500 \times 500$ μm) or 30 fps (FOV $\sim 250 \times 500$ μm). Furthermore, we demonstrate that this device possesses sufficient sensitivity to visualize fluorescent contrast agents topically applied or systemically delivered in animal and human tissues. No significant photobleaching was noted during the *in vivo* or *ex vivo* experiments.

3.1 *Experimental Characterization with Reflective Targets*

Axial-response measurements of the microscope, to a flat reflective mirror in a 5% Intralipid scattering phantom (or water), were performed over a range of depths [Figs. 2(a) and 2(b)], where depth is expressed here in terms of a nondimensional perpendicular optical length (L_P) as described in Section 2.2. The contrast (SBR: signal-to-background ratio) of the video-rate LS-DAC microscope in scattering media can be approximated as the ratio between the infocus signal (mirror located at $z = 0$) and the background signal (mirror located 15 to 20 μm away from $z = 0$). For example, the SBR is approximately 100 at a depth of $L_P = 4.4$, which is equivalent to a physical depth of $d = 200$ μm in our 5% Intralipid scattering phantom where $\mu_s \sim 11$ mm^{-1}. At shallow depths, the FWHM axial resolution for the microscope is 2.2 μm [Figs. 2(a) and 2(b)]. The reflectance images [Figs. 2(c) and 2(d)] demonstrate that the microscope can resolve group 8, element 5 of a USAF bar target, in which the line widths are 1.23 μm. The galvanometric scanning mirror introduces a slight field curvature (approximately 7 μm of axial displacement over a FOV of 500 μm in diameter) that results in the vignetting seen in Fig. 2(c). However, this slight curvature is not a significant problem when imaging within thick tissues.

3.2 *In Vivo Imaging of Blood Cells Trafficking within Capillaries*

Figure 3(a) shows a maximum-intensity projection of a z-stack of images collected at 30 fps (FOV of 250×500 μm) over a depth span of 125 to 200 μm beneath the surface of the mouse ear. The maximum-intensity projection displays the highest intensity from each z-column of pixels when projecting the entire z-stack of images onto a 2-D image (the projection is in the axial or z-direction). At an imaging rate of 30 fps, the motion of individual red blood cells within the capillaries of the mouse ear can be visualized (see Video 1, in which the microscope

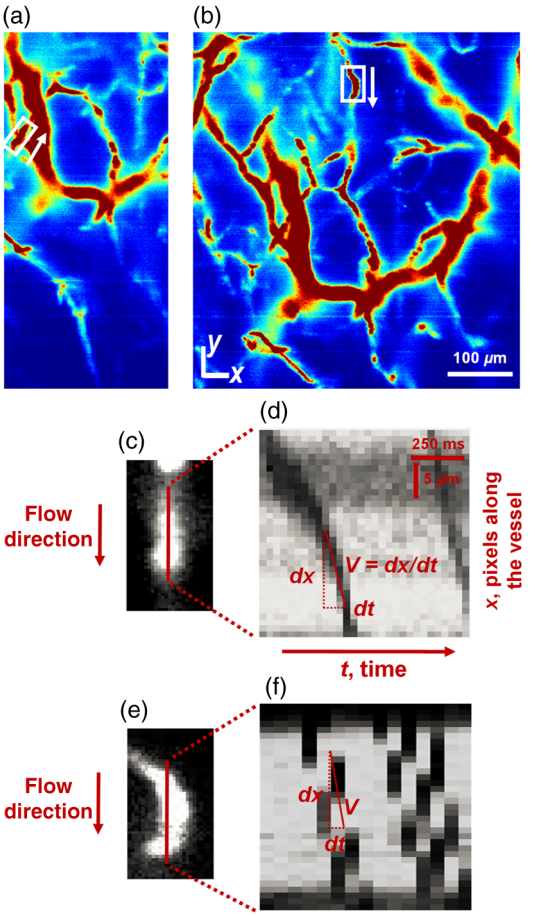

Fig. 3 A maximum-intensity projection (in the axial or *z*-direction) of a stack of images collected at depths ranging from $z = 125$ to 200 μm from the surface of a mouse ear at a frame rate of (a) 30 fps over a field of view (FOV) of 250×500 μm (Video 1) and (b) at 15 fps over a FOV of 500×500 μm (Video 2). (Video 1, MPEG, 389 KB [URL: http://dx.doi.org/10.1117/1.JBO.20.10.106011.1]; Video 2, MPEG, 2.3 MB [URL: http://dx.doi.org/10.1117/1.JBO.20.10.106011.2]). (c) and (e) Single-vessel images cropped from regions indicated in (a) and (b). The red lines indicate the locations where line-profile data are analyzed in panels (d) and (f) to quantify the velocity of the erythrocytes. The arrows indicate the direction of flow. The line profiles are arranged in the order of increasing time to calculate the velocity of the blood cells (see text for details). (d) Thirty line profiles from serially acquired images (with a frame rate of 30 fps). (f) Fifteen line profiles from serially acquired images (with a frame rate of 15 fps).

imaging depth is varied over time). Retro-orbitally injected FITC-dextran (2000 kDA molecular weight) illuminates the blood plasma while red blood cells can be observed as shadows trafficking through the capillaries. Serially acquired images can be analyzed to determine the velocity of the erythrocytes by observing a line profile centered along the length of a vessel.[35–37] For example, Fig. 3(d) shows 30 line profiles obtained over a total duration of 1 s (assuming a frame rate of 30 fps). The velocity is the ratio of the distance, d_x, traveled by a single red blood cell over a certain time interval, d_t, which is equivalent to the slope of the shadows seen in Figs. 3(d) and 3(f). The red blood cell velocities within the selected capillaries were calculated to be ~0.110 mm/s [Fig. 3(d)] and ~0.150 mm/s [Fig. 3(f)]. To image an FOV of 500×500 μm, the imaging frame rate was decreased to 15 fps [Fig. 3(b)]. However, the trafficking of red blood cells in capillaries could still be visualized and quantified (typical red blood cells velocity in the mouse ear capillaries is ~0.1 to 2 mm/s)[38] [see video 2 and Figs. 3(e) and 3(f)].

3.3 *Ex Vivo Imaging of Mouse Tongue*

Excised mouse tongue stained with methylene blue was fluorescently imaged at 15 fps over an FOV of $\sim 500 \times 500$ μm. The *ex vivo* image shown in Fig. 4(a)—acquired with a 100-μm line-acquisition rate, or 15-fps imaging rate—contains similar detail and contrast compared to the image of the same tissue in which a 1-ms line-acquisition rate (a 10× longer integration time) was utilized along with slow-stage scanning [Fig. 4(b)]. However, as shown in the example line profiles, there is a slight increase in noise for the high-speed image frame, as is expected due to lower photon counts at a 100-μs line-acquisition rate. The fungiform papillae (red arrow) and the numerous surrounding filiform papillae (blue arrows) are clearly visualized at a depth of 50 μm. Figure 4(c) shows a H&E stained histology section of a mouse tongue exhibiting similar structural details.

3.4 *Ex Vivo Imaging of Protoporphyrin IX-Expressing Human Brain Tumor*

Fluorescence imaging of thick (unsectioned) glioma tissues with LS-DAC microscopy at 15 fps [Fig. 5(a)] demonstrates adequate sensitivity to visualize subcellular PpIX expression (405-nm excitation and 625-nm collection), with similar structural details in comparison to fluorescence histopathology of PpIX, as shown in red in Fig. 5(b). Previous studies have already indicated the potential benefit of intraoperative confocal microscopy for guiding glioma resections.[39–41] However, the frame rates of previous devices have been insufficient to mitigate motion artifacts during handheld intraoperative use. Therefore, a miniature LS-DAC microscope, with a fast frame rate of 15 fps or higher, would be beneficial.

4 Discussion and Conclusion

In this study, video-rate imaging at 30 fps has been achieved with an LS-DAC microscope with sufficient speed, contrast, and sensitivity to visualize *in vivo* blood cell dynamics. In addition, high-speed LS-DAC microscopy at 15 fps provides sufficient sensitivity and contrast to visualize cellular details in tissues topically stained with a fluorescent contrast agent, methylene blue, as well as the subcellular expression of fluorescent PpIX in glioma tissues from patients administered with 5-ALA prior to surgery.

This is the first demonstration of *in vivo* video-rate imaging at 15 to 30 fps with a tabletop LS-DAC device, which provides an important benchmark for a miniature handheld LS-DAC microscope under development in our lab. Unlike previous LS-DAC prototypes that utilized slow-stage scanning, we have optimized the hardware, instrumentation, and software to achieve video-rate *in vivo* imaging. These results are a valuable step toward demonstrating the feasibility of an LS-DAC microscope for clinical applications, especially considering the low-NA collection optics utilized in a DAC microscope, in which the sensitivity for high-speed fluorescence detection has been unclear in the past. The results of this study suggest that LS-DAC microscopy has the potential to provide valuable functional and morphological information for point-of-care

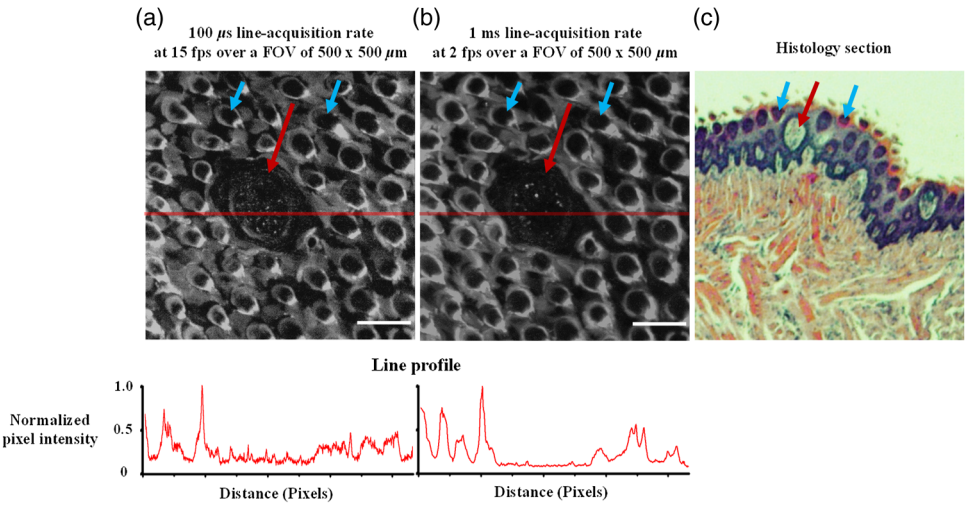

Fig. 4 (a) Excised mouse tongue stained with methylene blue and fluorescently imaged at (a) 15 fps over a FOV of ~500 × 500 μm, or imaged at (b) 2 fps over a FOV of ~500 × 500 μm. The normalized intensities of the pixels along the red band in (a) and (b) are plotted on the bottom. (c) H&E stained histology section of a mouse tongue. Scale bars = 100 μm.

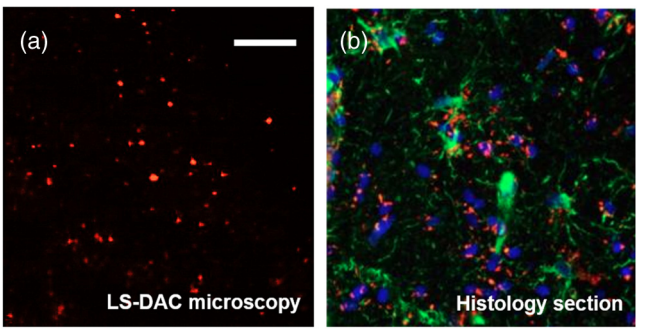

Fig. 5 (a) Surgically resected glioma (brain tumor) specimen fluorescently imaged at 15 fps over a FOV of ~500 × 500 μm. The patient was administered 5-aminolevulinic acid (5-ALA) prior to surgery. (b) A histological section of a similar glioma specimen from a patient administered with 5-ALA prior to surgery. The image shows DAPI-stained nuclei (blue), 5-ALA-induced protoporphyrin IX fluorescence (red), and the expression of glial fibrillary acidic protein (green). Scale bar = 100 μm.

cancer diagnostics and intraoperative guidance of tumor-resection procedures.

Acknowledgments

The authors acknowledge funding support from the NIH/NIDCR R01 DE023497 (Liu) and NCI R01 CA175391 (Liu and Sanai).

References

1. B. H. Zinselmeyer et al., "Video-rate two-photon imaging of mouse footpad-a promising model for studying leukocyte recruitment dynamics during inflammation," *Inflammation Res.* **57**, 93–96 (2008).
2. M. Akiba and K. P. Chan, "In vivo video-rate cellular-level full-field optical coherence tomography," *J. Biomed. Opt.* **12**(6), 064024 (2007).
3. I. Veilleux et al., "In vivo cell tracking with video rate multimodality laser scanning microscopy," *IEEE J. Sel. Top. Quantum Electron.* **14**, 10–18 (2008).
4. C. Halin et al., "In vivo imaging of lymphocyte trafficking," *Annu. Rev. Cell Dev. Biol.* **21**, 581–603 (2005).
5. M. Rajadhyaksha, R. R. Anderson, and R. H. Webb, "Video-rate confocal scanning laser microscope for imaging human tissues in vivo," *Appl. Opt.* **38**, 2105–2115 (1999).
6. C. L. Arrasmith, D. L. Dickensheets, and A. Mahadevan-Jansen, "MEMS-based handheld confocal microscope for in-vivo skin imaging," *Opt. Express* **18**, 3805–3819 (2010).
7. J. Eschbacher et al., "In vivo intraoperative confocal microscopy for real-time histopathological imaging of brain tumors," *J. Neurosurg.* **116**, 854–860 (2012).
8. K. Loewke et al., "Real-time image mosaicing with a hand-held dual-axes confocal microscope," *Proc. SPIE* **6851**, 68510F (2008).
9. R. Kiesslich et al., "Confocal laser endoscopy for diagnosing intraepithelial neoplasias and colorectal cancer in vivo," *Gastroenterology* **127**, 706–713 (2004).
10. T. D. Wang et al., "Dual-axis confocal microscope for high-resolution in vivo imaging," *Opt. Lett.* **28**, 414–416 (2003).
11. M. Rajadhyaksha et al., "In vivo confocal scanning laser microscopy of human skin: melanin provides strong contrast," *J. Invest. Dermatol.* **104**, 946–952 (1995).
12. J. G. Fujimoto, "Optical coherence tomography for ultrahigh resolution in vivo imaging," *Nat. Biotechnol.* **21**, 1361–1367 (2003).
13. W. Drexler et al., "In vivo ultrahigh-resolution optical coherence tomography," *Opt. Lett.* **24**, 1221–1223 (1999).
14. G. J. Tearney et al., "In vivo endoscopic optical biopsy with optical coherence tomography," *Science* **276**, 2037–2039 (1997).
15. L. An et al., "High speed spectral domain optical coherence tomography for retinal imaging at 500,000 Alines per second," *Biomed. Opt. Express* **2**, 2770–2783 (2011).
16. C. Stosiek et al., "*In vivo* two-photon calcium imaging of neuronal networks," *Proc. Natl. Acad. Sci. U. S. A.* **100**, 7319–7324 (2003).
17. J. Xi et al., "Integrated multimodal endomicroscopy platform for simultaneous en face optical coherence and two-photon fluorescence imaging," *Opt. Lett.* **37**, 362–364 (2012).
18. A. Zoumi, A. Yeh, and B. J. Tromberg, "Imaging cells and extracellular matrix in vivo by using second-harmonic generation and two-photon excited fluorescence," *Proc. Natl. Acad. Sci. U. S. A.* **99**, 11014–11019 (2002).
19. X. Wang et al., "Noninvasive laser-induced photoacoustic tomography for structural and functional in vivo imaging of the brain," *Nat. Biotechnol.* **21**, 803–806 (2003).
20. H. F. Zhang et al., "Functional photoacoustic microscopy for high-resolution and noninvasive in vivo imaging," *Nat. Biotechnol.* **24**, 848–851 (2006).
21. L. V. Wang and S. Hu, "Photoacoustic tomography: in vivo imaging from organelles to organs," *Science* **335**, 1458–1462 (2012).
22. J. M. Yang et al., "Optical-resolution photoacoustic endomicroscopy in vivo," *Biomed. Opt. Express* **6**, 918–932 (2015).

23. J. T. Liu et al., "Micromirror-scanned dual-axis confocal microscope utilizing a gradient-index relay lens for image guidance during brain surgery," *J. Biomed. Opt.* **15**(2), 026029 (2010).
24. W. Piyawattanametha et al., "In vivo near-infrared dual-axis confocal microendoscopy in the human lower gastrointestinal tract," *J. Biomed. Opt.* **17**(2), 021102 (2012).
25. S. Y. Leigh and J. T. Liu, "Multi-color miniature dual-axis confocal microscope for point-of-care pathology," *Opt. Lett.* **37**, 2430–2432 (2012).
26. J. T. Liu et al., "Efficient rejection of scattered light enables deep optical sectioning in turbid media with low-numerical-aperture optics in a dual-axis confocal architecture," *J. Biomed. Opt.* **13**(3), 034020 (2008).
27. A. Y. K. Chan, *Biomedical Device Technology: Principles and Design*, pp. 292–293, Charles C. Thomas, Illinois (2008).
28. R. W. Matthews and J. R. Matthews, *Insect Behavior*, pp. 275–276, Springer, Netherlands (2009).
29. D. Wang et al., "Comparison of line-scanned and point-scanned dual-axis confocal microscope performance," *Opt. Lett.* **38**, 5280–5283 (2013).
30. Y. Chen, D. Wang, and J. T. Liu, "Assessing the tissue-imaging performance of confocal microscope architectures via Monte Carlo simulations," *Opt. Lett.* **37**, 4495–4497 (2012).
31. D. Wang et al., "Sheet-scanned dual-axis confocal microscopy using Richardson–Lucy deconvolution," *Opt. Lett.* **39**, 5431 (2014).
32. Y. Chen and J. T. Liu, "Optimizing the performance of dual-axis confocal microscopes via Monte-Carlo scattering simulations and diffraction theory," *J. Biomed. Opt.* **18**(6), 066006 (2013).
33. W. Stummer et al., "Fluorescence-guided surgery with 5-aminolevulinic acid for resection of malignant glioma: a randomised controlled multicentre phase III trial," *Lancet Oncol.* **7**, 392–401 (2006).
34. D. Meza et al., "Comparing high-resolution microscopy techniques for potential intraoperative use in guiding low-grade glioma resections," *Lasers Surg. Med.* **47**, 289–295 (2015).
35. E. B. Brown et al., "In vivo measurement of gene expression, angiogenesis and physiological function in tumors using multiphoton laser scanning microscopy," *Nat. Med.* **7**, 864–868 (2001).
36. W. S. Kamoun et al., "Simultaneous measurement of RBC velocity, flux, hematocrit and shear rate in vascular networks," *Nat. Methods* **7**, 655–660 (2010).
37. T. N. Kim et al., "Line-scanning particle image velocimetry: an optical approach for quantifying a wide range of blood flow speeds in live animals," *PloS One* **7**, e38590 (2012).
38. M.-C. Zhong et al., "Trapping red blood cells in living animals using optical tweezers," *Nat. Commun.* **4**, 1768 (2013).
39. N. Sanai et al., "Intraoperative confocal microscopy in the visualization of 5-aminolevulinic acid fluorescence in low-grade gliomas," *J. Neurosurg.* **115**, 740–748 (2011).
40. J. T. Liu, D. Meza, and N. Sanai, "Trends in fluorescence image-guided surgery for gliomas," *Neurosurgery* **75**, 61–71 (2014).
41. N. Sanai et al., "Intraoperative confocal microscopy for brain tumors: a feasibility analysis in humans," *Neurosurgery* **68**, 282–290 (2011).

Ye Chen is a doctoral graduate student in the Mechanical Engineering Department at the University of Washington. She received her BS degree in applied mathematics and statistics and her MS degree in biomedical engineering from the State University of New York (SUNY) at Stony Brook.

Jonathan T. C. Liu is an assistant professor in the Mechanical Engineering Department at the University of Washington (UW), Seattle. He received his BSE degrees in mechanical engineering at Princeton in 1999 his MS and PhD degrees from Stanford in 2000 and 2005, respectively, followed by a postdoctoral fellowship in the Molecular Imaging Program at Stanford (2005–2009). Prior to joining UW, he was an instructor at the Stanford University School of Medicine and an assistant professor at SUNY Stony Brook (2010–2014).

Biographies for the other authors are not available.